# Pressure-Sensitive Multiple Superconducting Phases and Their Structural Origin in Van der Waals $HfS_2$ Up to 160 GPa

Wei Zhong,[1] He Zhang,[2,3] Ertugrul Karaca,[4,5] Jie Zhou,[1,6] Saori Kawaguchi,[7] Hirokazu Kadobayashi,[7] Xiaohui Yu,[2,3,8] Daniel Errandonea,[9] Binbin Yue,[1,*] and Fang Hong[2,3,8,†]

[1]*Center for High Pressure Science and Technology Advanced Research, 10 East Xibeiwang Road, Haidian, Beijing 100193, China*
[2]*Beijing National Laboratory for Condensed Matter Physics, Institute of Physics, Chinese Academy of Sciences, Beijing 100190, China*
[3]*School of Physical Sciences, University of Chinese Academy of Sciences, Beijing 100190, China*
[4]*Sakarya University, Biomedical, Magnetic, and Semiconductor Materials Research Center (BIMAS-RC), 54187 Sakarya, Turkey*
[5]*Center for Advanced Laser Techniques, Institute of Physics, 10000 Zagreb, Croatia*
[6]*Institute of Atomic and Molecular Physics, Sichuan University, Chengdu 610065, China*
[7]*SPring-8/JASRI, 1-1-1 Kouto, Sayo-gun, Sayo-cho, Hyogo 679-5198, Japan*
[8]*Songshan Lake Materials Laboratory, Dongguan, Guangdong 523808, China*
[9]*Departamento de Fisica Aplicada-ICMUV, MALTA Consolider Team, Universitat de Valencia, Avenue Doctor Moliner 50, 46100, Burjassot (Valencia), Spain*

(Received 28 March 2024; revised 25 June 2024; accepted 3 July 2024; published 9 August 2024)

Superconductivity has been observed in many insulating transition metal dichalcogenides (TMDCs) under pressure. However, the origin of superconductivity remains elusive due to the lack of studies on their structures at low temperatures. Here, we report the observation of a high-$T_c$ superconducting state (SC-I phase) coexisting with other superconducting states in a compressed $1T$-$HfS_2$ crystal up to approximately 160 GPa. *In situ* synchrotron x-ray diffraction results exclude the presence of decomposed sulfur and confirm two structural phase transitions at room temperature, as well as an additional transition at low temperature, which contribute to the emergence of multiple superconducting states. The SC-I phase exhibits an unsaturated $T_c$ of 16.4 K at 158 GPa, and demonstrates the highest upper critical field among the bulk TMDCs, $\mu_0 H_{c2}(0) \approx 29.7$ T for a $T_c \sim 15.2$ K at 147 GPa, exceeding the weak-coupling Pauli limit. These results reveal abundant SC properties together with sensitive structures in compressed $HfS_2$, and thereby extend our understanding on TMDCs' superconductivity.

DOI: 10.1103/PhysRevLett.133.066001

Transition metal dichalcogenides (TMDCs) have garnered broad attention due to their layered structure and exceptional electronic properties [1–4]. Pressure can enhance interlayer interactions in TMDCs, which finally induces significant structural or electronic transitions and even superconductivity [3–6]. $2H$-$MoS_2$ undergoes insulator-metal transition and becomes a superconductor through a pressure-driven isostructural transition [7]. Bulk $2H$-$TaS_2$ shows two superconducting (SC) phases under ultrahigh pressure while the restacked $TaS_2$ shows the highest $T_c$ and a large critical field at ~150 GPa in TMDCs [8,9]. Pressure-induced superconductivity has also been reported in $HfSe_2$ [10,11], $TiTe_2$ [12,13], $SnS_2$ [14]. However, the superconductivity looks very complicated under megabar pressure, since diverse superconductivity behavior can be observed in the same compound. $2H$-$TaS_2$ shows multiple SC transitions, and its SC-II phase with high $T_c$ shows some similarity with pure sulfur (both of them have similar $T_c$ and low critical field) [8]. Restacked $TaS_2$ shows a remarkable SC critical field, and it has the same $T_c$ with the bulk $TaS_2$ whose critical field is very small [8,9]. Recently, $1T$-$HfS_2$ was reported to demonstrate different superconductivity under ultrahigh pressure, as the bulk $HfS_2$ shows a $T_c \sim 12.2$ K at 173 GPa [15], while another work reports a $T_c$ of only 4.4 K at 153 GPa [16]. The significant discrepancy in a same TMDC compound suggests the possibility of complex phase transitions and SC states under high pressure and low temperature. In addition, there is no solid evidence to exclude the contribution of decomposed chalcogens, considering the similar $T_c$ in pure chalcogens and TMDCs. To address these issues, it is necessary and crucial to conduct detailed structural studies on TMDCs under high pressure and low temperature.

In this work, we conducted temperature-dependent synchrotron x-ray diffraction (XRD) and transport

*Contact author: yuebb@hpstar.ac.cn
†Contact author: hongfang@iphy.ac.cn

 © 2024 American Physical Society

measurements on $1T$-$HfS_2$ and observed a much higher $T_c$, close to 17 K, which is unsaturated in current pressure limit of 158 GPa. The SC transitions clearly show multiple stages, and show different responses to the external magnetic field. Low-temperature XRD excludes the existence of decomposed S, and provides evidence that multiple SC states in $HfS_2$ originate from the coexistence of $I4/mmm$ and $R\bar{3}m$ structure. Meanwhile, SC $HfS_2$ has a large upper critical field $\mu_0 H_{c2}(0)$ with $T_c \sim 15.2$ K at 147 GPa, reaching ~30 T by empirical fitting [or ~45 T using Ginzburg-Landau (G-L) formula fitting], the highest among bulk TMDCs. The exceptionally $\mu_0 H_{c2}(0)$ surpasses the weak-coupling Pauli limit ($\mu_0 H_p$). Apart from the Ising superconductivity observed only in single or few-layer TMDCs [17,18], $HfS_2$ stands out as the first bulk TMDC superconductor with such a high $\mu_0 H_{c2}(0)$. These results suggest the presence of unconventional superconductivity linked to novel structures in compressed $HfS_2$, and it is promising to explore unconventional superconductivity in similar 4f-electron systems. $HfS_2$ thus emerges as a valuable platform for investigating the interplay between unconventional superconductivity, structure, and electronic configurations.

The electrical transport experiments were conducted on a $1T$-$HfS_2$ single crystal. Sample characterizations (Fig. S1), experiments and theoretical calculations can be found in the Supplemental Material [19]. The resistance-temperature ($R$-$T$) curves under higher pressure are shown in Fig. 1. At low pressure range, $HfS_2$ remains a semiconductor until 73 GPa in Fig. S2 [19], consistent with the previous report [29]. Interestingly, a slight drop of resistance at 78 GPa is observed at a very low temperature in Fig. 1(a), indicating a SC transition. As pressure increases, the SC transition becomes more pronounced, and a zero-resistance state is observed at 147 GPa and 1.7 K. Figure 1(b) enlarges the view of $R$-$T$ curves below 20 K, clearly revealing the superconductivity with multiple transitions. A possible reason for the multiple transitions is the inhomogeneous superconductivity caused by the pressure gradient, which is shown in $HfS_3$ [30]. Another possible reason is that multiple SC states could be due to the coexistence of different phases. The multiple SC transitions can be seen clearly in the differential of resistance ($dR/dT$) in Fig. S3(a) [19]. Three SC states are named SC-I, SC-II, and SC-III, respectively. The $T_c^{\text{SC-I}}$ is enhanced by pressure monotonously, and the transition region becomes sharper and sharper. At the maximum pressure of 158 GPa, the $T_c^{\text{SC-I}}$ reaches 16.4 K, which is the highest record in TMDCs, the same as that in the compressed $2H$-$TaS_2$ [8]. If the $T_c^{\text{SC-I}}$ is defined by the crossing point of $dR/dT$ [31], as seen in Fig. S3(a) [19], it would be almost equal to the $T_c$(~17 K) of $\beta$-Po type S measured near 160 GPa [32]. The highest $T_c^{\text{SC-I}}$ is also higher than the previous $T_c$ record of 12.2 K for $1T$-$HfS_2$ [15]. In contrast, the $T_c^{\text{SC-II}}$(~11.4 K) at 158 GPa is closer to this old record [15].

Figure 2(a) illustrates low-temperature $R$-$T$ curves at 147 GPa under various magnetic fields. The $T_c$ clearly shifts to lower temperatures with the magnetic field, and zero resistance is also suppressed, which are typical features of SC transitions. The SC-I surprisingly persists under 8 T, while the SC-III is completely suppressed above 2 T. This behavior of SC-III under magnetic fields is very similar to the previous results in $HfS_2$ with a $T_c$ of 4 K [16]. As the magnetic field increases to 4 T, the SC-II also becomes indistinguishable. These different responses under various magnetic fields give complementary evidence of the multiple SC states, akin to $2H$-$TaS_2$ [8].

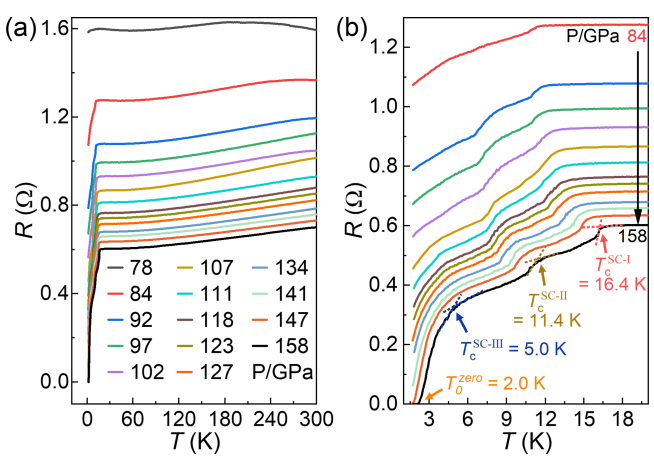


FIG. 1. The electrical transport properties of $HfS_2$ under ultrahigh pressure. (a) The $R$-$T$ curves of superconductivity, from 78 to 158 GPa. (b) The enlarged region of the SC transitions, and zero-resistance state can be seen clearly at 147 and 158 GPa. The multistage drops of resistance indicate the possibility of multiple SC states, and different colored arrows show their $T_c$.

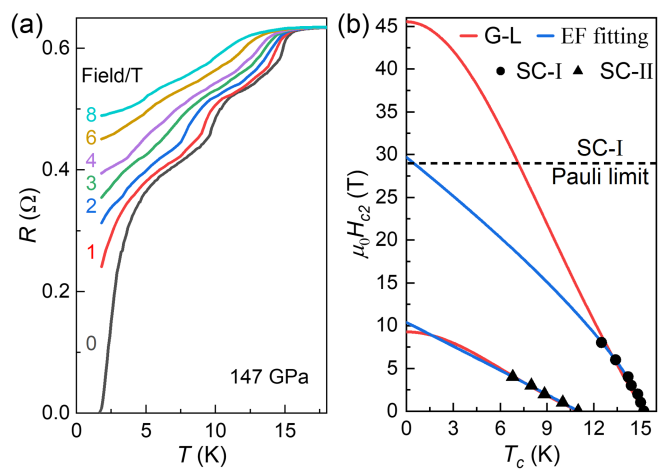


FIG. 2. The magnetic field effect on the SC transition in $HfS_2$ at 147 GPa. (a) The $R$-$T$ curves at various magnetic fields. (b) The relation between upper critical field and $T_c$, fitting by the Ginzburg-Landau (G-L) formula and empirical formula (EF) $H_{c2}(T) = H_{c2} \times (1 - T/T_c)^{1+\alpha}$.

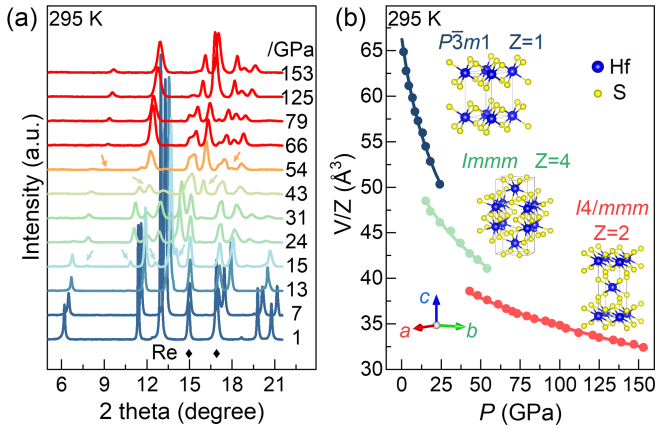


FIG. 3. High-pressure XRD results of $HfS_2$ at room temperature. (a) High-pressure powder XRD patterns obtained at 295 K. Phase transition features are indicated by arrows. (b) The pressure dependent volume per formula (V/Z) of three phases at 295 K (trigonal $P\bar{3}m1$ with a Z number of 1, orthorhombic $Immm$ with a Z number of 4, tetragonal $I4/mmm$ with a Z number of 2). The curves were fitted by third-order Birch-Murnaghan equation of state.

The $\mu_0 H_{c2}$ as a function of $T_c$ is plotted for SC-I and SC-II in Fig. 2(b), while such a relation for SC-III is not provided due to not enough data. The $\mu_0 H_{c2}(0)$ is fitted with the G-L formula and empirical formula (EF) $H_{c2}(T) = H_{c2} \times (1 - T/T_c)^{1+\alpha}$ [33]. Here, the parameter $\alpha$ itself does not have a specific physics meaning, but it can indicate the sensitivity of SC in magnetic fields. A larger $\alpha$ value corresponds to a higher critical field and weaker sensitivity of SC to external magnetic field. The fitted $\mu_0 H_{c2}(0)$ value of SC-II is $\sim$9.25 T(G-L) or $\sim$10.4 T(EF, $\alpha \approx 0.02$), and both of them are lower than the Pauli limit, $\mu_0 H_p \approx 1.84 T_c = 20.24$ T for $T_c \sim 11$ K. Most notably, the EF fitted $\mu_0 H_{c2}(0)$ of SC-I is $\sim$29.7 T($\alpha \approx 0.15$), which is higher than the Pauli limit, $\mu_0 H_p = 27.97$ T for $T_c \sim 15.2$ K. A much higher $\mu_0 H_{c2}(0) \approx 45.5$ T can be obtained with the G-L formula. In Fig. S4, the fitting based on $T_c$ values defined by the $dR/dT$ demonstrates the $\mu_0 H_{c2}(0)$ of SC-I exceeding the Pauli limit as well [19]. Furthermore, if using the Werthamer-Helfand-Hohenberg formula [34] $\mu_0 H_{c2}(0) = -0.693 T_c (d\mu_0 H_{c2}/dT)_{T=Tc}$ to estimate the orbital limit $\mu_0 H_{c2}(0)$ of SC-I, a much larger value of $\mu_0 H_{c2}^{\mathrm{orb}}(0) \sim 52.7$ T is obtained for $(d\mu_0 H_{c2}/dT)_{T=Tc} \sim -5$ T/K. Another magnetic field effect measurement was conducted at 107 GPa, as shown in Fig. S5 [19]. Two measurements share similar results, providing evidence for a large $\mu_0 H_{c2}(0)$ of SC-I and the distinct magnetic field responses for three SC states. The large $\mu_0 H_{c2}(0)$ surpassing Pauli limit means that it is hard to describe SC-I based on the weak-coupling Bardeen-Cooper-Schrieffer model, and it may be unconventional superconductivity.

To investigate the structure origin of multiple SC states in $HfS_2$ under ultrahigh pressure, high-pressure powder XRD is performed at both room (Fig. 3) and low temperature (Fig. 4). In Fig. 3(a), the first phase transition ($P\bar{3}m1$ to $Immm$) appears around 15 GPa, and the second phase transition ($Immm$ to $I4/mmm$) occurs at $\sim$43 GPa, consistent with Refs. [15,29]. $HfS_2$ remains a pure $I4/mmm$ phase from 66 to 153 GPa at 295 K. However, the ultrahigh pressure XRD patterns exhibit significant differences from another XRD result using a 4:1 methanol-ethanol mixture as pressure medium [16]. The ultrahigh pressure structures of that work are more likely to be a mixed state of $Immm$ and $I4/mmm$. This implies that different pressure conditions can induce distinct phase transition behaviors in $HfS_2$ under ultrahigh pressure. The Rietveld refined examples for three phases at 295 K are provided in Fig. S6, and the lattice parameters of three phases are plotted in Fig. S7 [19]. The volume per formula (V/Z) of the three

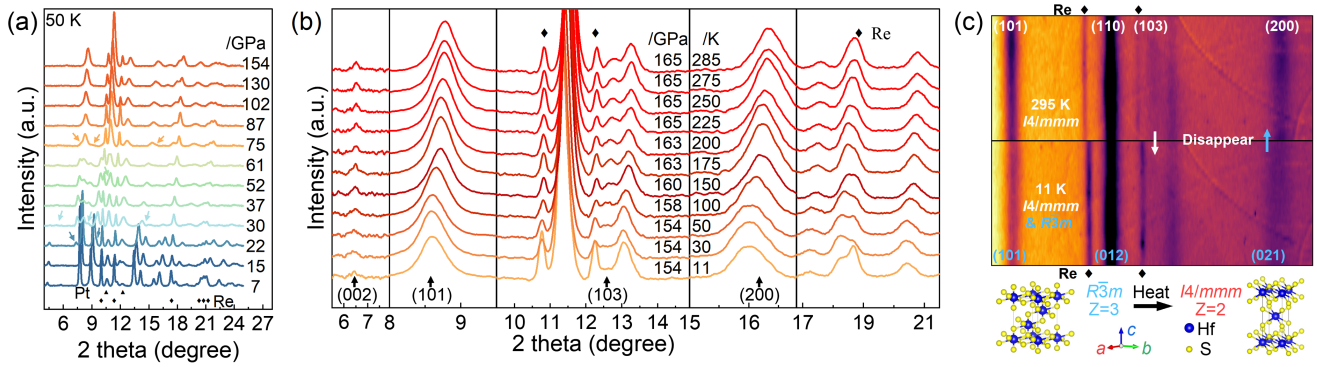


FIG. 4. High-pressure XRD results of $HfS_2$ at low temperatures. (a) High-pressure powder XRD patterns obtained at 50 K. (b) The XRD patterns obtained during the warming process at the highest pressure. The triangular and diamond symbols indicate peaks from platinum and rhenium, respectively. (c) The original diffraction patterns at 11 K (154 GPa) and 295 K (165 GPa), showing the phase transition features and the atomic structures of trigonal $R\bar{3}m$ and tetragonal $I4/mmm$ phases. To enhance the visual clarity, the diffraction peaks of $I4/mmm$ phase at 11 K and 295 K are aligned. The (103) peak in $I4/mmm$ phase is absent in $R\bar{3}m$ phase, and the (200) peak in $I4/mmm$ phase broadens toward lower diffraction angle at 11 K.

phases at 295 K were fitted by the third-order Birch-Murnaghan equation of state, as shown in Fig. 3(b). For ease of comparing the bulk modulus, we fixed $B_0'$ at 4. The resulting $V_0$ and $B_0$ for each phase are as follows: $V_0 = 66.3(3)$ Å$^3$, $B_0 = 51.63(19)$ GPa for $P\bar{3}m1$; $V_0 = 53.7(4)$ Å$^3$, $B_0 = 120(7)$ GPa for $Immm$; $V_0 = 42.9(2)$ Å$^3$, $B_0 = 315.7(7)$ GPa for $I4/mmm$.

Although the room-temperature XRD results show no additional phase transitions beyond 66 GPa, distinct phase transition trends emerge at low temperatures. The critical pressures for phase transitions at low temperature, such as 50 K, are higher compared with those at room temperature [Fig. 4(a)]. The first phase transition completes around 30 GPa, while the second phase transition emerges between 52 and 75 GPa. Above 80 GPa, low-temperature XRD patterns exhibited significant differences, particularly at 11 K and 154 GPa shown in Fig. 4(b). At these extreme conditions, the (002) and (103) peaks in $I4/mmm$ weaken, and a tendency of splitting and broadening emerges in the (101) and (200) peaks. This implies that the structures giving rise to SC-I and SC-II are not solely of the pure $I4/mmm$ phase but rather a mixed phase. As the temperature increases to 100 K, pure $I4/mmm$ structure gradually recovers, with all specific peaks reverting clearly. In Fig. 4(c), we compare the raw data corresponding to 11 K and 295 K to visualize the phase transition features in a much clearer way. The diffraction peaks of $I4/mmm$ phase at 11 K and 295 K have been almost aligned. Upon cooling, the (101) peak in $I4/mmm$ slightly shifts toward higher angles, but the (200) peak in $I4/mmm$ moves toward lower angle and becomes broader. Meanwhile, the (103) peak in $I4/mmm$ is not noticeable at 11 K. These outcomes suggest that $I4/mmm$ gradually transforms into a new structure with decreasing temperature. However, this phase transition remains incomplete at 154 GPa and 11 K, maintaining a coexistence of two phases. The coexisting phases hinder new structure identification, but the structural transition in other $AB_2$-type compounds with the $I4/mmm$ structure may provide valuable references. By referencing the phase transition of $BaC_2$ under pressure [35], we purposed that the new low-temperature structure adopt the space group $R\bar{3}m$. A schematic representation of $R\bar{3}m$ phase is illustrated in Fig. 4(c). The d spacing of (012) in $R\bar{3}m$ closely resembles that of (110) in $I4/mmm$. Hence, the structural transition might be triggered by atomic slip parallel to the (110) plane in $I4/mmm$. This slip disrupts the symmetry along the $c$ axis in $I4/mmm$, causing the disappearance of (001) and (013) peaks. The (101) and (021) peaks in $R\bar{3}m$ also align well with the previously observed low-temperature variations of (101) and (200) peaks in $I4/mmm$. Therefore, it is reasonable to assign the new structure as the $R\bar{3}m$ phase. The refinement of x-ray pattern for the coexisting phases at 154 GPa and 11 K is displayed in Fig. S8(c) [19].

Based on the experimental results, we propose the phase diagram shown in Fig. 5(a). It is clear that the critical pressures of phase transitions are different between room and low temperatures. After the complete disappearance of $Immm$ at ~80 GPa, the coexistence of $R\bar{3}m$ and $I4/mmm$ at low temperature leads to the emergence of SC-I and SC-II. By referring to the theoretical calculations [19] (the results will be discussed later) and previous studies on $HfS_2$ [15] and S [32,36,37], we attempt to allocate the SC-II to the $I4/mmm$ structure, while SC-I may be associated with the $R\bar{3}m$ structure. It is noted that the $\beta$-Po type S is also in form of $R\bar{3}m$ structure, and its highest $T_c$ is very close to that of SC-I of $HfS_2$. However, the $R\bar{3}m$ phase of $HfS_2$ has much larger lattice parameters [$a = 3.612(2)$ Å, $c = 5.616(3)$ Å at 154 GPa], compared to those in the $\beta$-Po type S [$a = 3.3780(1)$ Å, $c = 2.6919(3)$ Å at 160 GPa] [37], eliminating the possibility of $HfS_2$ dissociating into elemental S. As for the SC-III, regrettably, whether new phase transitions exist below 11 K remain unknown.

To understand the electronic behavior and the superconductivity in $HfS_2$, a systematic theoretical calculation on the band structures is performed and the results are displayed in Supplemental Material [19]. At low pressure, both $P\bar{3}m1$ (Fig. S9) and $Immm$ (Fig. S10) phases remain in a semiconducting state, consistent with our experimental results. Above 80 GPa, both $I4/mmm$ and $R\bar{3}m$ phases behave as a good metal. In $I4/mmm$ phase (Fig. S11), the density of states at the Fermi level is contributed by the S-3$p$, S-3$s$, and Hf-5$d$ electrons. For $R\bar{3}m$ phase

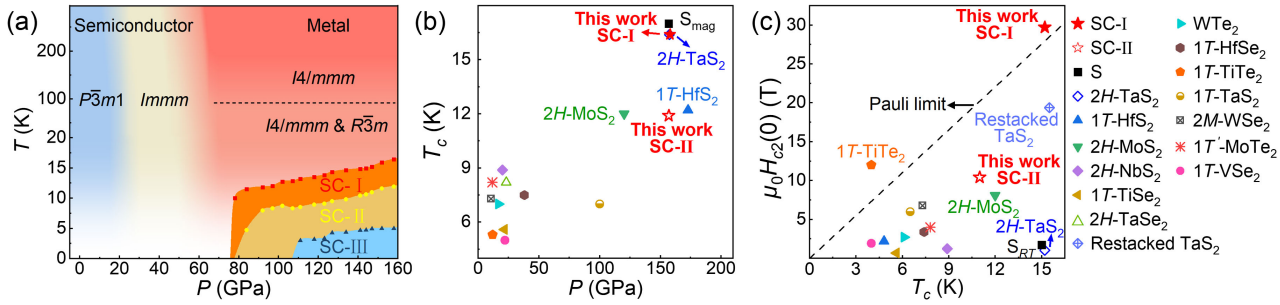


FIG. 5. Proposed phase diagram of $HfS_2$ (a), and the summarized $T_c$ (b), and $\mu_0 H_{c2}(0)$ (c) for different bulk TMDCs and sulfur. The $T_c$ of $S_{mag}$ and $S_{RT}$ are obtained from magnetic susceptibility and $R$-$T$ curves, respectively.

(Fig. S12), Hf-6s electrons made extra contribution to the density of states at Fermi level. In addition, some parameters for superconductivity, such as the electron-phonon coupling constant $\lambda$, logarithmic average phonon frequency $\omega_{ln}$, and theoretical $T_c$ values, are also calculated and the results are demonstrated in Table S1. The $T_c$ in both $I4/mmm$ and $R\bar{3}m$ phases increases monotonically with pressure, and $R\bar{3}m$ phase shows a higher $T_c$ than $I4/mmm$ *phase* at the same pressure. At 160 GPa, the calculated $T_c$ for $R\bar{3}m$ (~18.00 K) and $I4/mmm$ (~12.58 K) phases match well with the experimental values of the SC-I and SC-II phases, respectively. The multiband characteristic, due to the electron contribution of additional electron orbitals in Hf atoms at the Fermi level, may reveal the mechanism of the high $\mu_0 H_{c2}(0)$ observed in the $R\bar{3}m$ phase of $HfS_2$, different from $\beta$-Po type S [36]. Strong spin-orbit interaction may be another possible reason for the large $\mu_0 H_{c2}(0)$ of $R\bar{3}m$ phase. The $R\bar{3}m$ phase could possibly be described as $\beta$-Po type S doped with Hf atoms like metal hydrides. For heavy rare-earth elements near Hf, such as Yb and Lu, their hydrides exhibit a strong correlation between the 4f-electron states at the Fermi level and superconductivity [38]. According to Werthamer-Helfand-Hohenberg theory, the strong spin-orbit scattering would counteract the effects of the spin paramagnetism and then enhance the critical field [34]. The large atomic number of Hf with 4f electrons indicates the possibility of a strong spin-orbit interaction.

To demonstrate the interesting SC behavior in $HfS_2$ in a clear way, we summarize the SC features of compressed TMDCs in Figs. 5(b) and 5(c) [6–9,13,15,39–45]. Besides the highest $T_c$ (16.4 K), SC-I stands out with the largest $\mu_0 H_{c2}(0)$. Unlike the dome-shaped $T_c$ seen in $1T$-$HfS_2$ [15], $2H$-$TaS_2$ [8], and S [46], it is absent within the pressure limits in SC-I and SC-II [Fig. 5(a)], suggesting the potential for $HfS_2$ to create a higher $T_c$ record in TMDCs. $HfS_2$ becomes an alternative system showing promising unconventional superconductivity apart from the $1T$-$TiTe_2$, which also surpasses the $\mu_0 H_p$ due to the possible multiband superconductivity [13]. The special SC behavior also further distinguishes SC-I from previous studies on $HfS_2$ [15,16]. This distinction is likely attributed to variations in the pressure gradient effect induced by different pressure media of NaCl [15], KBr (this work), and no media [16]. The smaller bulk modulus of KBr than NaCl in the $B2$ ($Pm3m$) phase provides better hydrostatic conditions [47,48], while a no medium environment is considered as a uniaxial pressure condition. Such discrepancies might result in different phase transitions or physical properties, as seen in examples like $WTe_2$ [42], $TiSe_2$ [41,49], and $TiTe_2$ [13].

In summary, we report the multiple SC transitions in $1T$-$HfS_2$ combined with *in situ* low-temperature synchrotron XRD up to ~160 GPa. The coexistence of $I4/mmm$ and $R\bar{3}m$ in the low-temperature XRD results, coupled with the different response to the magnetic field observed in the SC resistance drop, collectively corroborate the existence of the multistep superconductivity. This also rules out the possibility of superconductivity induced by elemental sulfur. The highest $T_c \sim 16.4$ K in SC-I is observed at 158 GPa, and a large $\mu_0 H_{c2}(0) \sim 30$ T is obtained for a $T_c \sim 15.2$ K at 147 GPa. Because of the violation of the weak-coupling Pauli limit, it may be an unconventional superconductor, which is worthy of further study. Such a high $T_c$ of SC-I equals the previous record observed in $2H$-$TaS_2$ and restacked $TaS_2$. Contrary to the saturation trend of $T_c$ in $TaS_2$, the $T_c$ in SC-I of this study is unsaturated, hinting at the potential for achieving a higher $T_c$ under higher pressure. Importantly, the superconductivity in $HfS_2$ sets a new record for bulk TMDCs due to its large $\mu_0 H_{c2}(0)$. These exciting results show us the abundant transport behavior and sensitive structures of $HfS_2$ under high pressure, and opens a new window for us to study the novel superconductivity in other TMDC compounds.

*Acknowledgments*—This work was supported by the National Key Research and Development Program of China (Grant No. 2021YFA1400300), the Major Program of National Natural Science Foundation of China (Grant No. 22090041), the National Natural Science Foundation of China (Grants No. 12004014, No. U1930401, No. 12374050). Part of the experimental work was carried out at the Synergic Extreme Conditions User Facility. The room-temperature XRD was performed at the BL15U beamline of the Shanghai Synchrotron Radiation Facility (SSRF). The low-temperature XRD was supported by Super Photon ring-8 (SPring-8) and conducted at the BL10XU beamline (Proposal No. 2023B1412). D. E. thanks the support from Spanish AEI and Spanish MCIN: Grants No. PID2022-138076NB-C41 and No. RED2022-134388-T cofinanced by EUFEDER funds (DOI: 10.13039/501100011033), GVA: Grants No. CIPROM/2021/075 and No. MFA/2022/007, and Advanced Materials Program supported by MCIN and GVA with NextGenerationEU funds PRTR-C17.I1.

B. Y. and F. H. conceived the project. F. H., W. Z., H. Z., and X. H. Y. did the transport measurement. W. Z., B. Y., F. H., J. Z., H. Z., S. K., and H. K. conducted the low-temperature high-pressure x-ray diffraction experiments. E. K. and D. E. did the theoretical calculation. W. Z., B. Y., and F. H. analyzed the data and wrote the manuscript. All authors made comments on the manuscript and have given approval to the final version of the manuscript.

[1] S. Paul, S. Talukdar, R. S. Singh, and S. Saha, Topological phase transition in $MoTe_2$: A review, Phys. Status Solidi RRL **17**, 2200420 (2023).

[2] D. Qiu, C. Gong, S. Wang, M. Zhang, C. Yang, X. Wang, and J. Xiong, Recent advances in 2D superconductors, Adv. Mater. **33**, 2006124 (2021).

[3] L. Zhang, Y. Tang, A. R. Khan, M. M. Hasan, P. Wang, H. Yan, T. Yildirim, J. F. Torres, G. P. Neupane, Y. Zhang *et al.*, 2D materials and heterostructures at extreme pressure, Adv. Sci. **7**, 2002697 (2020).

[4] S. Pei, Z. Wang, and J. Xia, High pressure studies of 2D materials and heterostructures: A review, Mater. Des. **213**, 110363 (2022).

[5] B. Sipos, A. F. Kusmartseva, A. Akrap, H. Berger, L. Forró, and E. Tutiš, From Mott state to superconductivity in $1T$-$TaS_2$, Nat. Mater. **7**, 960 (2008).

[6] Q. Dong, Q. Li, S. Li, X. Shi, S. Niu, S. Liu, R. Liu, B. Liu, X. Luo, J. Si *et al.*, Structural phase transition and superconductivity hierarchy in $1T$-$TaS_2$ under pressure up to 100 GPa, npj Quantum Mater. **6**, 20 (2021).

[7] Z. Chi, X. Chen, F. Yen, F. Peng, Y. Zhou, J. Zhu, Y. Zhang, X. Liu, C. Lin, S. Chu *et al.*, Superconductivity in pristine $2H_a$-$MoS_2$ at ultrahigh pressure, Phys. Rev. Lett. **120**, 037002 (2018).

[8] Q. Dong, J. Pan, S. Li, Y. Fang, T. Lin, S. Liu, B. Liu, Q. Li, F. Huang, and B. Liu, Record-high superconductivity in transition metal dichalcogenides emerged in compressed $2H$-$TaS_2$, Adv. Mater. **34**, 2103168 (2022).

[9] Q. Dong, J. Pan, S. Li, C. Li, T. Lin, B. Liu, R. Liu, Q. Li, F. Huang, and B. Liu, Abnormal metal–semiconductor-like transition and exceptional enhanced superconducting state in pressurized restacked $TaS_2$, J. Am. Chem. Soc. **145**, 14581 (2023).

[10] S. Rahman, H. Saqib, X. Liang, D. Errandonea, A. S. Resta, A. Molina-Sanchez, G. Gao, L. Wang, Y. Tian, and H. K. Mao, Pressure-induced metallization and robust superconductivity in pristine $1T$-$HfSe_2$, Mater. Today Phys. **25**, 100698 (2022).

[11] C. Tian, Y. Gao, F. Tian, X. Wang, Z. Zhang, D. Duan, X. Huang, and T. Cui, Dimensionality switching and superconductivity transition in dense $1T$-$HfSe_2$, Phys. Rev. B **105**, L180506 (2022).

[12] Y. Zhou, C. Chen, Y. Zhou, X. Chen, C. Gu, C. An, B. Zhang, Y. Yuan, H. Wu, R. Zhang *et al.*, Pressure-induced evolution of structural and electronic properties in $TiTe_2$, Phys. Rev. B **99**, 125104 (2019).

[13] U. Dutta, P. S. Malavi, S. Sahoo, B. Joseph, and S. Karmakar, Pressure-induced superconductivity in semimetallic $1T$-$TiTe_2$ and its persistence upon decompression, Phys. Rev. B **97**, 060503(R) (2018).

[14] B. Yue, W. Zhong, X. Yu, and F. Hong, Superconductivity in the van der Waals crystal $SnS_2$ up to 105 GPa, Phys. Rev. B **105**, 104514 (2022).

[15] S. Rahman, L. Wang, H. Saqib, D. Errandonea, L. Yang, Y. Zhao, Y. Zhuang, G. Gao, L. Wang, and Y. Tian, Metallization and superconductivity with $T_c > 12$ K in transition metal dichalcogenide $HfS_2$ under pressure, Mater. Today Phys. **34**, 101091 (2023).

[16] S. Zhang, H. Wang, H. Liu, J. Zhen, S. Wan, W. Deng, Y. Han, B. Chen, and C. Gao, Superconductivity in $HfS_2$ at ultrahigh pressure, Phys. Rev. Mater. **7**, 104802 (2023).

[17] S. Foner and E. J. McNiff, Upper critical fields of layered superconducting $NbSe_2$ at low temperature, Phys. Lett. **45A**, 429 (1973).

[18] X. Xi, Z. Wang, W. Zhao, J.-H. Park, K. T. Law, H. Berger, L. Forró, J. Shan, and K. F. Mak, Ising pairing in superconducting $NbSe_2$ atomic layers, Nat. Phys. **12**, 139 (2016).

[19] See Supplemental Material at http://link.aps.org/supplemental/10.1103/PhysRevLett.133.066001, which includes Refs. [20–28], for experimental methods, sample characterizations, the $T_c$ defined by differential of resistance at low temperature, other $\mu_0 H_{c2}(0)$ fitting examples, the XRD Rietveld refinements, and the computational detail.

[20] P. Giannozzi, S. Baroni, N. Bonini, M. Calandra, R. Car, C. Cavazzoni, D. Ceresoli, G. L. Chiarotti, M. Cococcioni, I. Dabo *et al.*, Quantum espresso: A modular and open-source software project for quantum simulations of materials, J. Phys. Condens. Matter **21**, 395502 (2009).

[21] P. Giannozzi, O. Andreussi, T. Brumme, O. Bunau, M. Buongiorno Nardelli, M. Calandra, R. Car, C. Cavazzoni, D. Ceresoli, M. Cococcioni *et al.*, Advanced capabilities for materials modelling with quantum espresso, J. Phys. Condens. Matter **29**, 465901 (2017).

[22] J. P. Perdew, K. Burke, and M. Ernzerhof, Generalized gradient approximation made simple, Phys. Rev. Lett. **77**, 3865 (1996).

[23] A. M. Rappe, K. M. Rabe, E. Kaxiras, and J. D. Joannopoulos, Optimized pseudopotentials, Phys. Rev. B **41**, 1227 (1990).

[24] A. B. Migdal, Interaction between electrons and lattice vibrations in a normal metal, Sov. Phys. JETP **7**, 996 (1958), http://83.149.229.155/cgi-bin/dn/e_007_06_0996.pdf.

[25] G. Eliashberg, Interactions between electrons and lattice vibrations in a superconductor, Sov. Phys. JETP **11**, 696 (1960), http://jetp.ras.ru/cgi-bin/dn/e_011_03_0696.pdf.

[26] P. B. Allen and R. C. Dynes, Transition temperature of strong-coupled superconductors reanalyzed, Phys. Rev. B **12**, 905 (1975).

[27] P. B. Allen and R. C. Dynes, Superconductivity at very strong coupling, J. Phys. C **8**, L158 (1975).

[28] H. M. Tütüncü, H. Y. Uzunok, E. Karaca, G. P. Srivastava, S. Özer, and Ş. Uğur, Ab initio investigation of BCS-type superconductivity in $LuNi_2B_2C$-type superconductors, Phys. Rev. B **92**, 054510 (2015).

[29] W. Zhong, W. Deng, F. Hong, and B. Yue, Structural and electronic phase transition in the van der Waals crystal $HfS_2$ under high pressure, Phys. Rev. B **107**, 134118 (2023).

[30] B. Yue, W. Zhong, W. Deng, T. Wen, Y. Wang, Y. Yin, P. Shan, J.-T. Wang, X. Yu, and F. Hong, Insulator-to-superconductor transition in quasi-one-dimensional $HfS_3$ under pressure, J. Am. Chem. Soc. **145**, 1301 (2023).

[31] L. Gao, Y. Y. Xue, F. Chen, Q. Xiong, R. L. Meng, D. Ramirez, C. W. Chu, J. H. Eggert, and H. K. Mao, Superconductivity up to 164 K in $HgBa_2Ca_{m-1}Cu_mO_{2m+2+\delta}$ ($m = 1$, 2, and 3) under quasihydrostatic pressures, Phys. Rev. B **50**, 4260 (1994).

[32] V. V. Struzhkin, R. J. Hemley, H.-k. Mao, and Y. A. Timofeev, Superconductivity at 10–17 K in compressed sulphur, Nature (London) **390**, 382 (1997).

[33] K. H. Müller, G. Fuchs, A. Handstein, K. Nenkov, V. N. Narozhnyi, and D. Eckert, The upper critical field in superconducting $MgB_2$, J. Alloys Compd. **322**, L10 (2001).

[34] N. R. Werthamer, E. Helfand, and P. C. Hohenberg, Temperature and purity dependence of the superconducting critical field, $H_{c2}$. III. electron spin and spin-orbit effects, Phys. Rev. **147**, 295 (1966).

[35] I. Efthimiopoulos, K. Kunc, G. V. Vazhenin, E. Stavrou, K. Syassen, M. Hanfland, S. Liebig, and U. Ruschewitz, Structural transformation and vibrational properties of $BaC_2$ at high pressure, Phys. Rev. B **85**, 054105 (2012).

[36] S. Kometani, M. I. Eremets, K. Shimizu, M. Kobayashi, and K. Amaya, Observation of pressure-induced superconductivity of sulfur, J. Phys. Soc. Jpn. **66**, 2564 (1997).

[37] O. Degtyareva, E. Gregoryanz, H. K. Mao, and R. J. Hemley, Crystal structure of sulfur and selenium at pressures up to 160 GPa, High Press. Res. **25**, 17 (2005).

[38] H. Song, Z. Zhang, T. Cui, C. J. Pickard, V. Z. Kresin, and D. Duan, High Tc superconductivity in heavy rare earth hydrides, Chin. Phys. Lett. **38**, 107401 (2021).

[39] S. Sahoo, U. Dutta, L. Harnagea, A. K. Sood, and S. Karmakar, Pressure-induced suppression of charge density wave and emergence of superconductivity in $1T$-$VSe_2$, Phys. Rev. B **101**, 014514 (2020).

[40] Y. Fang, Q. Dong, J. Pan, H. Liu, P. Liu, Y. Sun, Q. Li, W. Zhao, B. Liu, and F. Huang, Observation of superconductivity in pressurized 2M $WSe_2$ crystals, J. Mater. Chem. C **7**, 8551 (2019).

[41] W. Xia, J. Wu, Z. Li, J. Yuan, C. An, X. Wang, N. Yu, Z. Zou, G. Liu, C. Zhou *et al.*, Pressure-induced superconductivity reentrant in transition metal dichalcogenide $TiSe_2$, arXiv:2202.06244.

[42] X.-C. Pan, X. Chen, H. Liu, Y. Feng, Z. Wei, Y. Zhou, Z. Chi, L. Pi, F. Yen, F. Song *et al.*, Pressure-driven dome-shaped superconductivity and electronic structural evolution in tungsten ditelluride, Nat. Commun. **6**, 7805 (2015).

[43] Y. Qi, P. G. Naumov, M. N. Ali, C. R. Rajamathi, W. Schnelle, O. Barkalov, M. Hanfland, S.-C. Wu, C. Shekhar, Y. Sun *et al.*, Superconductivity in Weyl semimetal candidate $MoTe_2$, Nat. Commun. **7**, 11038 (2016).

[44] D. C. Freitas, P. Rodière, M. R. Osorio, E. Navarro-Moratalla, N. M. Nemes, V. G. Tissen, L. Cario, E. Coronado, M. García-Hernández, S. Vieira *et al.*, Strong enhancement of superconductivity at high pressures within the charge-density-wave states of $2H$-$TaS_2$ an $2H$-$TaSe_2$, Phys. Rev. B **93**, 184512 (2016).

[45] V. G. Tissen, M. R. Osorio, J. P. Brison, N. M. Nemes, M. García-Hernández, L. Cario, P. Rodière, S. Vieira, and H. Suderow, Pressure dependence of superconducting critical temperature and upper critical field of $2H$-$NbS_2$, Phys. Rev. B **87**, 134502 (2013).

[46] E. Gregoryanz, V. V. Struzhkin, R. J. Hemley, M. I. Eremets, H. K. Mao, and Y. A. Timofeev, Superconductivity in the chalcogens up to multimegabar pressures, Phys. Rev. B **65**, 064504 (2002).

[47] A. Dewaele, A. B. Belonoshko, G. Garbarino, F. Occelli, P. Bouvier, M. Hanfland, and M. Mezouar, High-pressure–high-temperature equation of state of KCl and KBr, Phys. Rev. B **85**, 214105 (2012).

[48] N. Sata, G. Shen, M. L. Rivers, and S. R. Sutton, Pressure-volume equation of state of the high-pressure $B2$ phase of NaCl, Phys. Rev. B **65**, 104114 (2002).

[49] H. Saqib, S. Rahman, Y. Zhao, C. Cazorla, D. Errandonea, R. Susilo, Y. Zhuang, y. Huang, B. Chen, and N. Dai, Evolution of structural and electronic properties of $TiSe_2$ under high pressure, J. Phys. Chem. Lett. **12**, 9859 (2021).